Multifunctional Silver-Exchanged Zeolite Micromotors for Catalytic Detoxification of Chemical and Biological Threats

*Virendra V. Singh, Beatriz Jurado-Sánchez, Sirilak Sattayasamitsathit, Jahir Orozco, Jinxing Li, Michael Galarnyk, Yuri Fedorak, and Joseph Wang**

Multifunctional reactive-zeolite-based micromotors have been developed and characterized toward effective and rapid elimination of chemical and biological threats. The incorporation of silver ions (Ag^+) into aluminosilicate zeolite framework imparts several attractive functions, including strong binding to chemical warfare agents (CWA) followed by effective degradation, and enhanced antibacterial activity. The new zeolite-micromotors protocol thus combines the remarkable adsorption capacity of zeolites and the efficient catalytic properties of the reactive Ag^+ ions with the autonomous movement of the zeolite micromotors for an accelerated detoxification of CWA. Furthermore, the high antibacterial activity of Ag^+ along with the rapid micromotor movement enhances the contact between bacteria and reactive Ag^+, leading to a powerful "on-the-fly" bacteria killing capacity. These attractive adsorptive/catalytic features of the self-propelled zeolite micromotors eliminate secondary environmental contamination compared to adsorptive micromotors. The distinct cubic geometry of the zeolite micromotors leads to enhanced bubble generation and faster movement, in unique movement trajectories, which increases the fluid convection and highly efficient detoxification of CWA and killing of bacteria. The attractive capabilities of these zeolite micromotors will pave the way for their diverse applications in defense, environmental and biomedical applications in more economical and sustainable manner.

1. Introduction

There have been growing recent concerns about the possible use of deadly chemical warfare agents (CWA) by terrorist groups. Therefore, detoxification of such deadly nerve agents in battlefield and civilian conditions presents a major technological challenge and continues to be of considerable national security interest.[1] Current methods for the decontamination of CWA involve the use of strong oxidants,[2] enzymatic biodegradation,[3] atmospheric pressure plasma,[4] photocatalytic,[5] and incineration methods.[6] These procedures have their own drawbacks, such as lack of stability (loss of activity over time), strong environmental impact, and high temperature, which make them unsuitable for large-scale field-based detoxification of CWA. On-going studies thus aim at developing environmentally friendly and cost-effective strategies for destroying chemical-weapon stockpiles in field locations without endangering humans or the environment.

In order to address the drawbacks associated with the aforementioned process, several environmentally friendly inorganic solid adsorbents have been explored for the decontamination applications;[7–10] however, due to lack of reactivity even after several days such adsorbents may lead to secondary contamination to the environment. To overcome these drawbacks, reactive sorbents, particularly exchanged zeolites, are of great interest because of their remarkable high surface area and catalytic activity toward CWA detoxification.[11,12]

Similarly to CWA, biological warfare agents (BWA) and other life threatening outbreak of infectious diseases caused by different pathogenic bacteria, require efficient protocols for effective and rapid killing of bacteria. Over the past decades, the potential benefits of silver materials have attracted tremendous attention of scientific communities due to the strong antibacterial activity against a broad spectrum of bacteria, viruses, and fungi.[13,14] The antibacterial properties of silver species depend largely upon the contact of bacteria with silver species.[15–17]

We describe here a novel detoxification method based on self-propelled multifunctional silver-exchanged zeolite micromotors for effective detoxification of chemical and biological threats. Synthetic nano/micromotors have opened a new horizon for the scientific community due to their diverse practical applications ranging from biomedical[18] to environmental remediation.[19] Self-propelled micromotors based on different reactive materials have shown considerable promise for accelerating decontamination processes. The effective movement of remediation materials through the contaminated water systems has led to new "move and destroy" remediation protocols, with higher efficiency and speed and potentially lower costs.[19] In order to develop a cost effective, environmentally friendly

Dr. V. V. Singh, Dr. B. Jurado-Sánchez,
Dr. S. Sattayasamitsathit, Dr. J. Orozco,
J. Li, M. Galarnyk, Y. Fedorak, Prof. J. Wang
Department of Nanoengineering
University of California
San Diego, La Jolla, CA 92093, USA
E-mail: josephwang@ucsd.edu

DOI: 10.1002/adfm.201500033

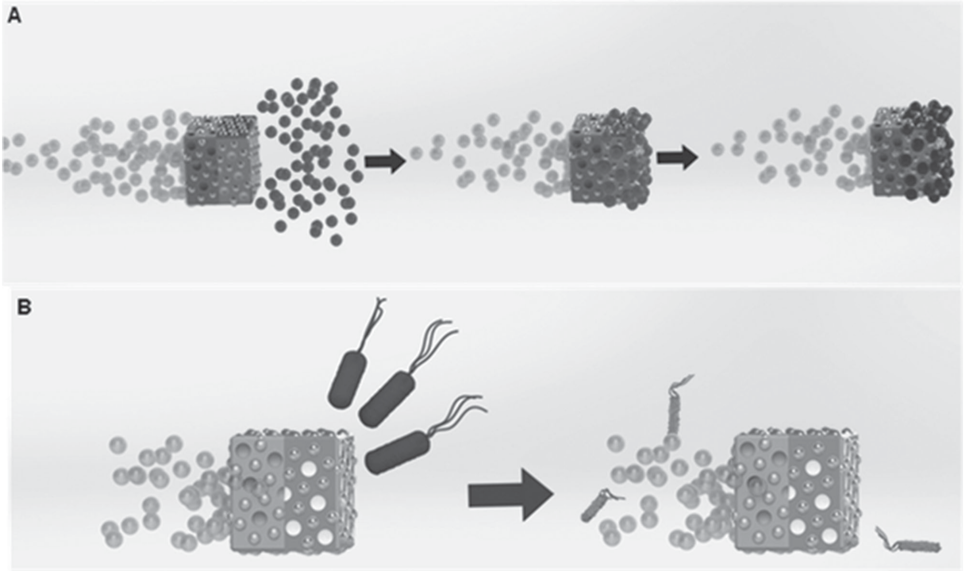

Figure 1. Zeolite micromotors with effective "on-the-fly" CWA degradation and antibacterial activity. Schematic representation of the self-propulsion of Ag-Z micromotors and their A) adsorptive/catalytic detoxification of CWA to environmentally-friendly products and B) powerful bacteria (*E. coli*) killing capacity.

and fast adsorptive/catalytic detoxification platform, special emphasis has been given to the selection of appropriate reactive materials.

Zeolites are microporous materials that consist of a 3D arrangement of $[SiO_4]^{4-}$ and $[AlO_4]^{5-}$ polyhedra connected through their oxygen atoms to form large negative lattices. The application of zeolite materials for environmental remediation has gained major attention due to their selective sorption capacities, non-toxic nature, availability, and low cost.[20a] Moreover, due to presence of 3D cage structure of zeolite, it has been widely used for the slow release of ions such as silver.[20b,c] As will be illustrated below, coupling the unique remediation properties of reactive zeolites with their autonomous propulsion through a contaminated sample leads to attractive new capabilities and significant advantages.

The multi-tasking capability of the new zeolite micromotors has been achieved by combining their efficient movement (and corresponding fluid convection) with the remarkable adsorption capacity of zeolites and the effective catalytic action of Ag^+ species on the 3D matrices of zeolites. Such "on-the-fly" adsorption/catalytic action and CWA detoxification action is shown to be very fast when compared to analogous static silver ion-exchanged zeolite (Ag-Z) systems. We also combined here the advantages of antibacterial properties of reactive Ag^+ with self-propelled motion toward improved detoxification of biological threats. Such enhanced capability is illustrated for the rapid killing of Gram-negative *E. coli* bacteria used as a BWA surrogate for plague bacteria.[21] Given the significant cost of Pt, we rely here on the use of silver as a catalyst for propelling the new zeolite motors by decomposition of H_2O_2 fuel and demonstrate the advantages of cube-shaped micromotors over common spherical micromotors. Peroxide-powered propulsion of silver-based micromotors has been described recently.[22] The new multifunctional Ag-Z micromotors offer cost effective, environmentally friendly, highly stable, and rapid dual detoxification of CWA and BWA without the need of common harsh environments, irradiating light and decontaminating reagents.[1,2,23] Such attractive capabilities of the Ag-Z-based micromotors are illustrated in the following sections for the detoxification of the CWA simulant diethyl chlorophosphate (DCP) and of the BWA surrogate *E. coli* bacteria (**Figure 1**).

2. Results and Discussion

The multifunctional-engineered Ag-Z micromotors architecture consists of high reactive Ag^+ embedded within the pores of the zeolite and asymmetric deposition of a catalytic silver patch on the outer surface of Ag-Z for the autonomous movement of micromotors. The molecular dimensions of the zeolite cages and channels prevent aggregation of Ag^+ into larger nanoparticles (because of steric reasons), thus it retains its higher reactivity.[24] Figure 1 illustrates a scheme of the self-propelled Ag-Z micromotors-based detoxification of CWA (A) and *E. coli* (B). Self-propelled Ag-Z micromotors perform"on-the-fly" detoxification of the nerve agent to environmentally friendly products that involves adsorption of CWA in the micropore and mesopore cavities of high surface-area zeolite for its further enhanced detoxification (Figure 1A). Detoxification is achieved by the aluminosilicate framework-hosted reactive Ag^+-assisted catalysis that promotes nucleophilic substitution and subsequent hydrolysis by entrapped water molecules. While Ag^+ can be released very slowly from the zeolite surface,[20b,c] such released Ag^+ contributes also to the hydrolysis of CWA. The micromotor displays efficient movement after long periods (>1 h) compared to the short (10 min) decontamination process, indicating that the slow release of Ag^+ is not a concern.

The reactive Ag^+-catalyzed hydrolysis along with the efficient solution mixing associated with the movement of cubic micromotors (without mechanical stirring) resulted in a significantly

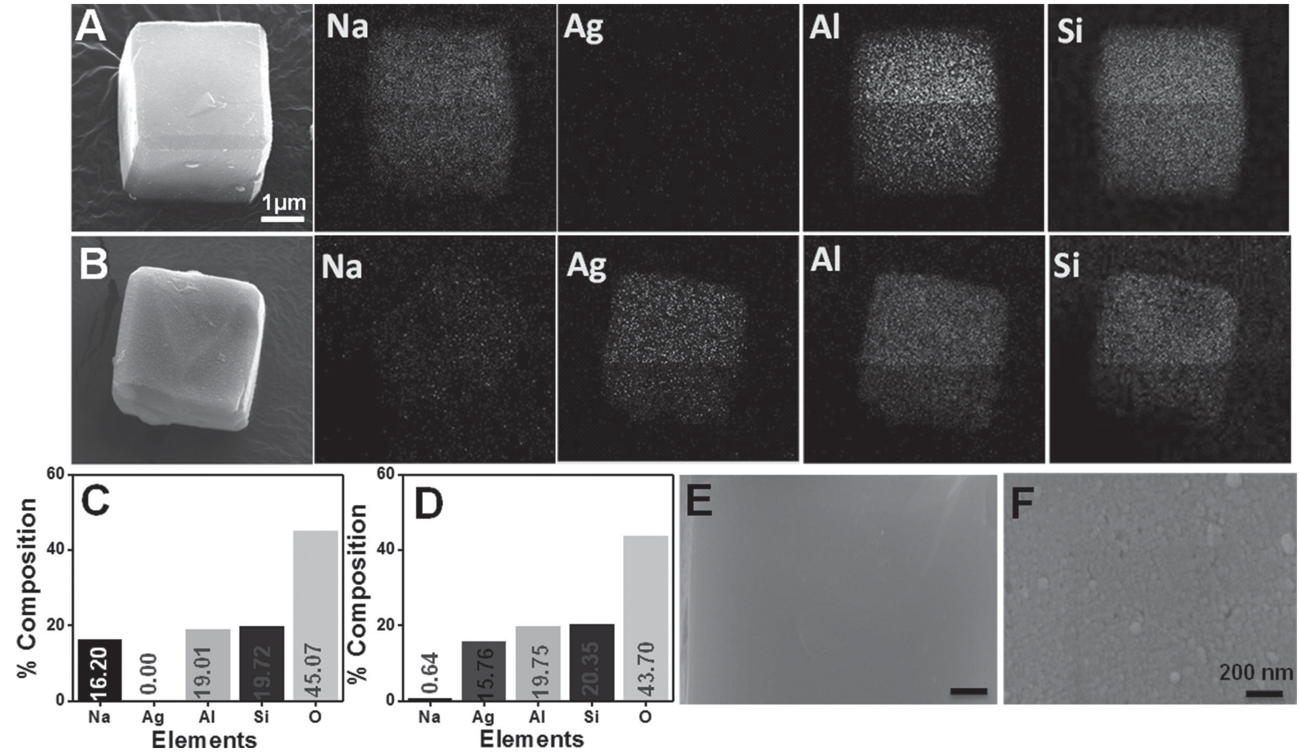

Figure 2. Scanning electron microscopy (SEM) images and energy-dispersive X-ray (EDX) spectroscopy images showing the different elements of the A) sodium zeolite and B) silver-ion-exchanged zeolite, along with C,D) elemental analysis; E) adsorptive face of the silver-ion-exchanged zeolite and F) Ag-nanoparticle catalytic layer on the surface of silver-exchanged zeolite for propulsion.

enhanced CWA detoxification process. Similarly, the self-propulsion of the Ag^+-containing micromotors promotes the effective interaction of the highly reactive Ag^+ species with an *E. coli* population towards rapid cell damage and death (Figure 1B).

The Ag-Z was prepared from the corresponding sodium zeolite (Na-Z) using a conventional ion-exchange procedure with an aqueous solution of silver nitrate at room temperature (Figure S1, Supporting Information). Scanning electron microscopy (SEM) images and energy-dispersive spectroscopic (EDX) mapping of the Na-Z and synthesized Ag-Z are shown in **Figure 2**A,B, respectively. These changes clearly illustrate the absence of Ag^+ before the ion-exchange reaction (Figure 2A), while showing the presence of Ag^+ and a very small amount of remaining Na^+ ion left after the ion-exchange treatment. EDX was also performed to determine the extent of Ag^+ exchange in the Na-Z and found it to be a 96% exchange. The content of Ag^+ in the exchanged zeolite was 15.8% (by weight) (Figure 2D). Comparison of EDX bar graphs of Na-Z (Figure 2C) versus Ag-Z (Figure 2D) indicates a nearly 1:1 exchange ratio of Na^+ to Ag^+; this implies that most of the counterion sites were occupied by Ag^+ without affecting the crystal structure of zeolite. X-ray diffraction (XRD) studies (Figure S3, Supporting Information) were also performed to examine the quality of synthesized Ag-Z and found that both (the exchanged and unexchanged zeolites) have similar XRD patterns, indicating that the zeolite retained its crystal structure after the Ag^+ exchange. These two analytical techniques (EDX and XRD) together provide evidence of the synthesis of the desired high-quality Ag-Z. Figure 2E,F display the adsorption and propulsion face of the Ag-Z micromotors, respectively.

The replacement of platinum with catalytic silver for the operation of micromotors was reported recently by Pumera's team in connection to the development of low-cost silver-based micromotors.[22] **Figure 3**A,B displays time-lapse images, taken from video 1 and video 2 (Supporting Information), illustrating the movement of the Ag-Z micromotor in pure water. A long, high-density tail of oxygen microbubbles is generated and ejected from the sputtered silver surface, which leads to an efficient bubble thrust and enhanced fluid transport. The Ag-Z micromotors are self-propelled at an ultrafast speed of 450 ± 100 μm s^{-1} with the typical curved (Figure 3A), circular, and self-rotating trajectories (Figure 3B). As anticipated, the speed of the Ag-Z micromotors is strongly dependent on the peroxide fuel concentration. The speed increases from 120 ± 25 to 250 ± 30 and 450 ± 100 μm s^{-1} using 1%, 2%, and 5% fuel concentrations, respectively.

The new zeolite micromotors can operate efficiently in raw real-life environmental samples and maintain high speeds in such media. The images in Figure S4A (Supporting Information) and the corresponding video S1 (Supporting Information) illustrate the efficient movement of multiple Ag-Z micromotors in untreated lake water at a high speed of 250 ± 50 μm s^{-1} (≈30 body lengths per second). The trajectory of the micromotors was not altered by the lake water matrix (90%, v/v), indicating the potential of Ag-Z micromotors for practical environmental applications. We have also compared the speed of cubic Ag-Z versus that of spherical (polystyrene-based) micromotors (video S2, Supporting Information) (Figure S4B, Supporting Information) under similar conditions. For example, the Ag-Z

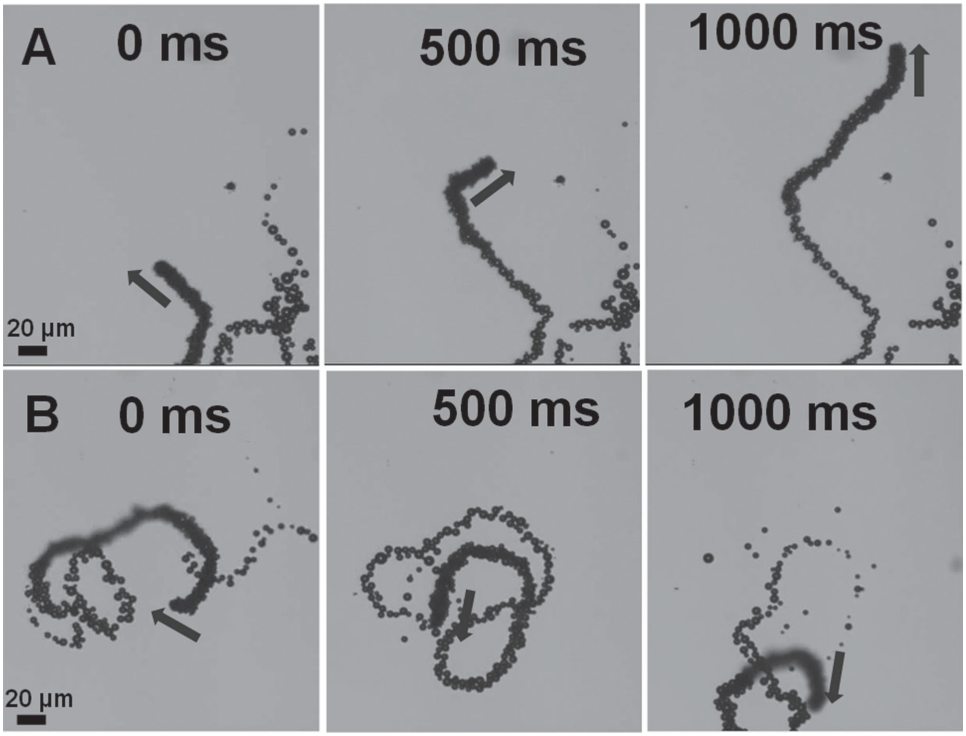

Figure 3. Motion of self-propelled Ag-Z micromotors. Time-lapse images at 500 ms intervals, showing the A) curved motion (taken from Video 1, Supporting Information) and B) circular and self-rotating motion (taken from Video 2, Supporting Information) of Ag-Z micromotor in ultrapure water in the presence of 5% H_2O_2 and 1% (w/v) SDS.

micromotor displays a speed of 250 µm s^{-1} (at a 2% peroxide level), compared to 80 µm s^{-1} for a similar size nonporous polystyrene micromotor (8 µm). This behavior can be explained by the combined effect of the cubic geometry, and porosity of Ag-Z micromotor (with the latter leading to a high number of bubble nucleation sites compared to the nonporous surface). Future studies (beyond the scope of this decontamination study) should involve comparison of motors of different shapes and porosities that may lead to new and improved propulsion behavior. Next, we moved our effort to examine the ability of Ag-Z micromotors to neutralize chemical threats. Due to safety requirements and government regulations related to the use of actual CWA, the reactive nerve agent simulant DCP has been used in this study since it displays a parallel reactivity to nerve agents such as sarin, soman, and tabun (Figure S2, Supporting Information).[26] The removal efficiency of nerve agent simulant DCP in the presence of Ag-Z micromotors was monitored spectrophotometrically by measuring the absorbance of the fluoresceinamine isomer-I (dye) at 475 nm after its interaction with DCP. The DCP phosphorylates the aromatic amine of fluoresceinamine isomer-I and forms an adduct (phosphoramide) and releases hydrochloric acid, which results in a decrease in the absorbance signal of the dye. Thus, higher concentrations of DCP molecules result in a larger decrease in absorbance signal of the fluoresceinamine isomer-I.

Optimization studies were performed prior to the remediation testing. As displayed in Figure S5 (Supporting Information) to optimize the amount of micromotors for the removal of 1×10^{-3} M DCP solution, different amounts of Ag-Z micromotors (1×10^6 to 5×10^6 micromotors mL^{-1}) were propelled for 6 min in a 1 mL contaminated solution. The absorbance spectra of Figure S5A (Supporting Information) shows that the extent of DCP removal increases from 25% to 90% upon increasing the density of Ag-Z micromotors from 1×10^6 to 5×10^6 micromotors mL^{-1}. Figure S5B (Supporting Information) displays the influence of the remediation time upon the removal of DCP over the 1 to 6 min range (1 min intervals) using the optimized amount of micromotors (5×10^6 micromotors mL^{-1}). It is observed that the DCP content decreased with increased remediation time and motor numbers.

After the optimization studies, the remediation experiments of DCP were carried out by immersing a known amount of the micromotors in 1 mL of contaminated solution. The micromotors were propelled in the contaminated solution for 6 min. A series of control experiments was also performed (**Figure 4**A-c, A-d) in a similar fashion, in order to elucidate the effect and role of the different solution components and processes involved in the accelerated CWA removal efficiency offered by the Ag-Z micromotors. As shown in Figure 4A-b, a small decrease in absorbance signal of fluoresceinamine isomer-I is observed, indicating the presence of a small amount of DCP after the Ag-Z micromotors-based remediation process, which corresponds to 90% removal. The driving force for the adsorption is diffusion gradient and convection induced by the micromotors, which lead to a higher adsorption rate. In contrast, a dramatic decrease of the dye absorbance signal is observed in control experiments (Figure 4A) involving static Ag-Z (Figure 4A-c) or moving Al_2O_3-Ag-Z (Figure 4A-d), reflecting the presence of most of the remaining threat in the solution (corresponding to 9.82% and 4.38% DCP removal, respectively). This can be

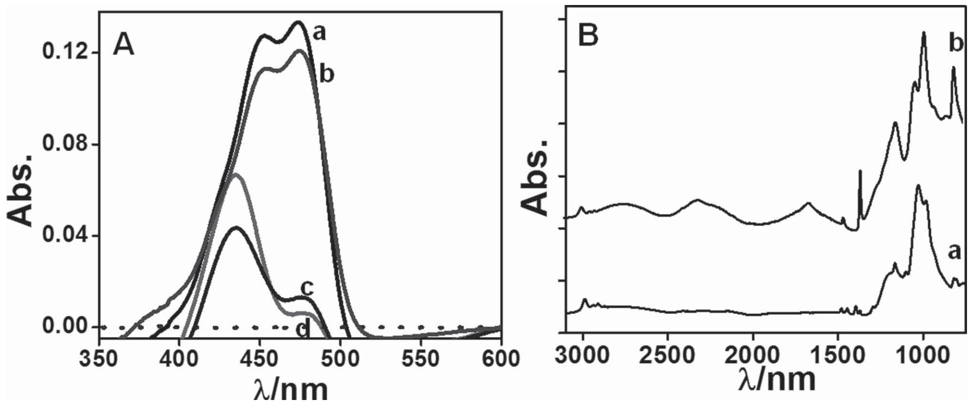

Figure 4. "On-the-fly" adsorptive detoxification of CWA using Ag-Z micromotors. A) Absorbance spectra of the fluoresceinamine (Co = 0.5×10^{-3} M) (a), after a 6-min treatment of DCP with moving Ag-Z micromotors (b), along with control experiments using static Ag-Z (c), and moving Al_2O_3-Ag-Z micromotors (d). B) FT-IR spectra of the product obtained at the surface of Na-Z micromotors (a) and Ag-Z micromotors (b). Conditions: 1 mL of 1.0×10^{-3} M DCP contaminated solution, containing 5×10^6 micromotors, 2% H_2O_2, and 1% SDS.

attributed to blocking of the accessible Ag and zeolite pores by the aluminum layer; DCP molecules are thus unable to access the pores of the silver ion-exchanged zeolite surface.

All data clearly indicates that the presence of micropores, mespores, and high surface area of the zeolite facilitates the adsorption of DCP molecules within the pores and retention of the nerve agent on the zeolite surface. The presence of Ag^+ leads to stronger interactions and accelerated chemisorption process. Moreover, the molecular size of the CWA was also found to play an important role on their adsorption over the Ag-Z micromotors. DCP has a molecular diameter of 12 Å size while sarin has a diameter of 7.04 Å (Table S1, Supporting Information).[27] The pore size of the Ag-Z varies from 5 to 20 Å.[28] Therefore, the DCP molecule is expected to be easily entrapped within the 3D matrix of Ag-Z micromotors. Nevertheless, it is also important to note that in zeolites, if molecules are larger than the pore aperture, the zeolite can flex slightly to enable the passage to molecules.[29]

In order to study the kinetics of adsorptive removal of DCP on the moving Ag-Z micromotors, static Ag-Z and moving Al_2O_3-Ag-Z micromotors, we plotted the log of residual amount of DCP, i.e., log (remaining DCP concentration) against the reaction time (t) (Figure S6, Supporting Information). The rate constant (K) was calculated using the slope of the straight line and half-life ($t_{1/2}$) was determined by 0.693 K^{-1}. The linear curves indicate that the reaction follows first-order rate equation. Results showed that the initial adsorption of DCP was faster, which is attributed to the rapid physisorption of DCP and then chemisorption due to the presence of Ag^+ species.[30] Table S3 (Supporting Information) displays the kinetics parameters for the adsorptive removal of DCP. These kinetics rate constant results indicate that the adsorption onto the moving Ag-Z micromotors is very fast when compared to the control static Ag-Z or moving Al_2O_3-Ag-Z micromotors.

The degradation product of DCP over moving Ag-Z and moving Na-Z micromotors was investigated by Fourier transform infrared (FT-IR) spectroscopy; the resultant IR band positions are listed in Table S4 (Supporting Information). In the case of Na-Z micromotor, the bands at 2990 cm^{-1} and 2940 cm^{-1} correspond to $–O–CH_2$ and $–CH_3$ asymmetric stretching, respectively. Also, the bands at 2875, 1485, 1370, 1165, 990, and 1030 cm^{-1} correspond to $–CH_2$ symmetric stretching; $–CH_3$ asymmetric bending; $O–CH_2$ deformation asymmetric vibration; $\nu P{=}O$ stretching vibration; P–O symmetric stretching, and δ(P–O–C) vibration, respectively.[31–33] While in the case of Ag-Z micromotors, the peaks at 2985 and 2740 cm^{-1} correspond to $–O–CH_2$ asymmetric stretching; and $–CH_3$ asymmetric stretching, respectively, and the characteristic P–OH band appears at 2300 cm^{-1}. The medium intensity bands at 1631, 1318, 1105, 980 and 932 cm^{-1} are assigned to the P(O)(OH) group; $O–CH_2$ deformation asymmetric vibration; $\nu P{=}O$ stretching vibration; P–O symmetric stretching; 932 cm^{-1} –P–OH asymmetric stretching, respectively. In the case of Ag-Z micromotors, we observed a slight shift in the band position of P(O)(OH) group; of the $O–CH_2$ deformation asymmetric vibration, the $\nu P{=}O$ stretching vibration and of the P–O symmetric stretching, compared to Na-Z micromotors (Table S4, Supporting Information); these shifts are attributed to the specific interaction of Ag^+ with the DCP molecule (Table S4, Supporting Information). These FT-IR findings confirm the hydrolysis of DCP molecules on the surface of Ag-Z micromotors and also support the catalytic degradation by Ag^+, when compared to Na-Z micromotors.

Based on the FT-IR data, a proposed mechanism for the adsorptive detoxification of DCP is shown in **Scheme 1**. When the moving Ag-Z micromotors come in contact with DCP, rapid adsorption and distribution of DCP molecules occurs within the accessible pores of Ag-Z due to physisorption; DCP then starts reacting with the active species Ag^+ ion available on the 3D matrix of zeolite. This leads to chemisorption or destruction of the DCP toxicant to such an extent that the chemical integrity of DCP is completely destroyed. The nucleophilic Ag-Z oxygen interacts with a carbon of one of the ethyl groups of one of the sides of the DCP molecule and Ag^+ counterion interacts with the ethyl ester oxygen atom and –Cl atom present in the DCP molecules.

The interaction between the Ag^+ counterion and oxygen atom polarizes the ester C–O bond, leading to an ethyl elimination and dehalogenation reaction. Meanwhile, as depicted in Scheme 1, the OH^- from water attacks the electrophilic center

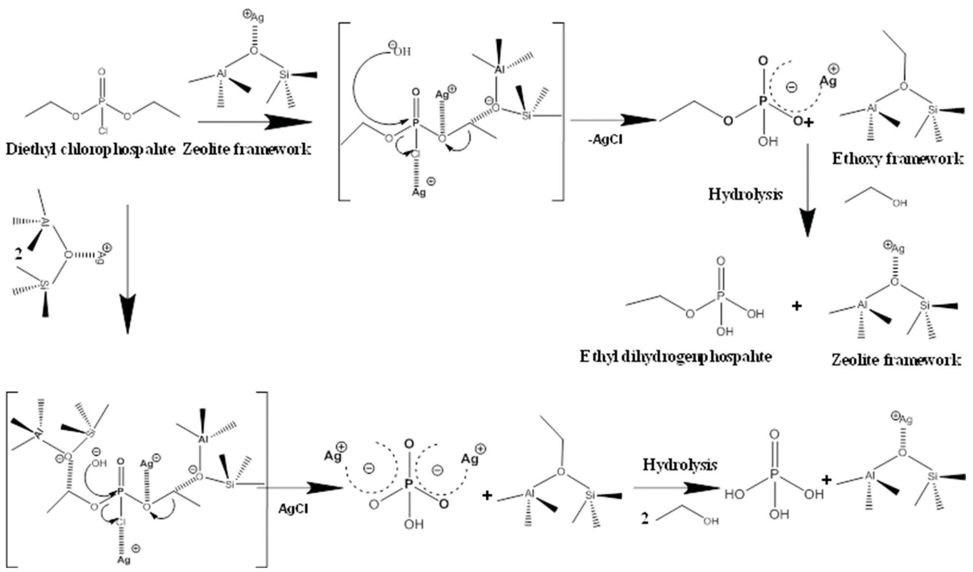

Scheme 1. Proposed reaction mechanism for the hydrolytic conversion of DCP into hydrolysis products on Ag-Z micromotors.

of the P=O bond and the Ag^+ ion is replaced by a H^+ ion and forms ethyl dihydrogen phosphate. The other possibility is that two nucleophilic Ag^+-exchanged zeolitic oxygen interact with both carbons of a DCP molecule and after subsequent hydrolysis it forms phosphoric acid. Thus, the formation of the environmentally friendly product ethyl dihydrogen phosphate or phosphoric acid involves hydrolysis and dehalogenation reactions at room temperature.

The versatility of the catalytic Ag-Z micromotors was also investigated towards the rapid killing of *E. coli* (Gram-negative strain DH5α) used as a BWA surrogate for plague bacteria. Among the other antibacterial agents, silver has been reported to be the most effective agent due to its ability to alter or interfere with many different functions of bacterial cells and is also nonselective in its antibacterial action.[34–37] While in the metallic state silver is inert, ionized silver is highly reactive as it binds to tissue proteins, nuclear membranes, and bacterial cell walls, leading to cell distortion and death.[38–40] These experiments were performed by immersing 5×10^6 Ag-Z micromotors in 1 mL of contaminated solution containing 1×10^8 cells mL^{-1} for 6 min. After the killing process, fluorescent imaging was used to evaluate the live and killed *E. coli*. Syto-9 dye (green) was used to label all the live and dead *E. coli,* while propidiumiodidepropidium iodide dye (red) was used to label the only the dead *E. coli*. **Figure 5**A-D shows fluorescence images of a) total *E. coli* (in green) and b) dead *E. coli* (in red).

In order to explain the efficacy of moving Ag-Z micromotors (Figure 5A), different control experiments were carried out using the same time period, including the use of static Ag-Z (Figure 5B), moving Na-Z micromotors (Figure 5C), and moving Al_2O_3-Ag-Z micromotors (Figure 5D). As illustrated in Figure 5B–D, negligible bacteria killing (ranging from 3.16% to 11.4%), is observed in all control experiments over the 6 min operation. In contrast, a significant (87.5%) antibacterial activity against *E. coli* was achieved with the moving Ag-Z micromotors over the same period, reflecting the efficient motion-induced antibacterial properties (compared to the static Ag-Z). Figure 5E illustrates the killing of *E. coli* by the micromotor-accelerated treatment as compared with control experiments in water after 6 min. A statistical plot was also made (Figure 5F) showing the comparative statistics of live and dead bacteria. The limited access of the reactive Ag^+ species to the bacteria in the absence of micromotors (or with static motors) is dramatically pronounced; however, this can be overcome when these reactive motors are actively swimming in the bacteria-contaminated solution. SEM studies were also conducted to confirm the above observations and to gain further insights into the killing of *E. coli*. Figure 5 shows SEM images of *E. coli* before (G) and after (H) the 6-min treatment with moving Ag-Z micromotors. These images clearly illustrate the dramatic change of the morphology and structure of the bacteria cell following the Ag-Z micromotors treatment. The wrinkled cell wall may reflect leakage of cytoplasmic contents outside the bacterial cell.[40]

3. Conclusion

We have demonstrated the use of catalytic silver-exchanged zeolite micromotors for a highly efficient "on-the-fly" accelerated detoxification strategy of both chemical and biological threats under mild conditions. The dramatically accelerated detoxification of CWA by the new zeolite-micromotor protocol reflects the combination of the remarkable adsorption capacity of zeolites with the efficient catalytic properties of embedded Ag^+ and the dynamic movement of the micromotors. Each component of the new zeolite micromotors thus has a specific function, making these zeolite-based micromotors practically operational, sustainable, economical, and environmentally friendly. These properties and capabilities make the zeolite micromotors advantageous over recently developed remediation motors. The directional motion of silver-exchanged zeolite micromotor in contaminated solution along with the high-density bubble tail, increases greatly the fluid transport, and leads to enhanced and accelerated detoxification and to green degradation products.

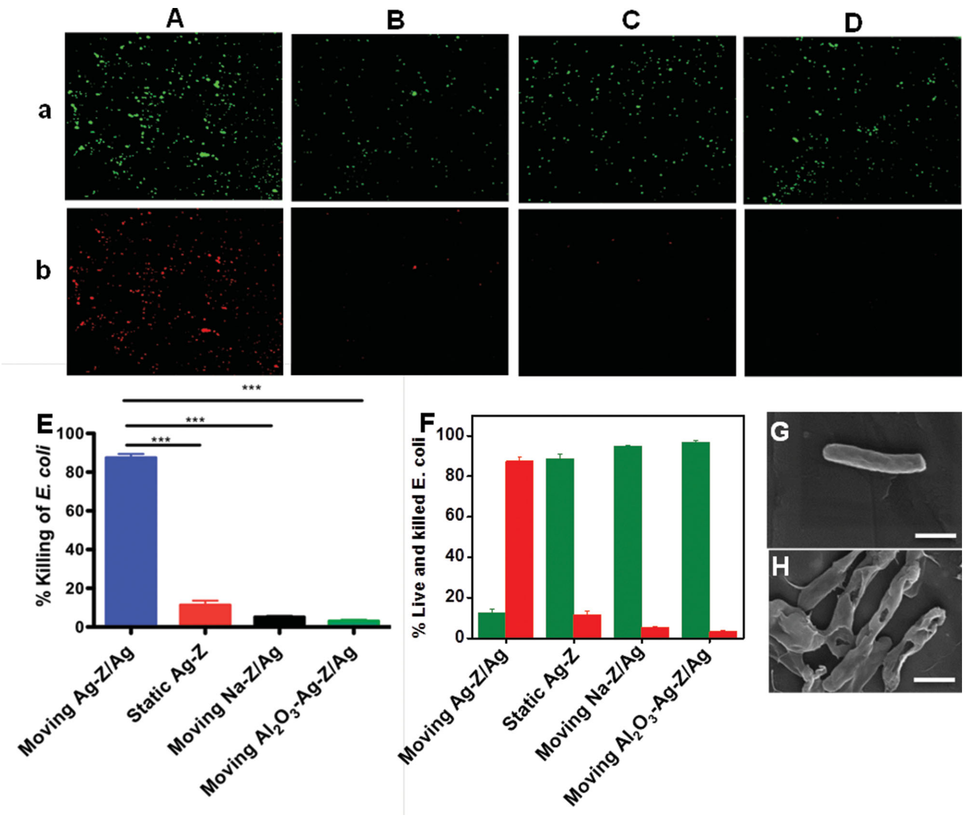

Figure 5. Ag-Z micromotors driven killing of *E. coli*, along with different control experiments. Fluorescence images of a) total *E. coli* in green color and b) dead *E. coli* in red color after a 6-min treatment of A) moving Ag-Z micromotors, B) static Ag-Z, C) moving Na-Z micromotors, and D) moving Al_2O_3-Ag-Z micromotors. E) Efficacy of Ag-Z micromotors with the control was assayed by its ability to kill the bacteria. Data are means ± SD ($n = 3$), Student's t-test, $p < 0.05$,*** denotes significantly different from other control. F) Statistical plot showing the *E. coli* killing efficiency by the Ag-Z micromotors and different control treatments; G) SEM images of the live *E. coli*, and of H) dead *E. coli* inactivated by the moving Ag-Z micromotors. Scale bar, 1 µm. Other conditions: total volume of the contaminated solution = 1 mL (containing 2% H_2O_2 and 1% SDS, motor number = 5×10^6 and a 6-min remediation time.

Future improvements in adsorptive detoxification reactivity may be achieved by tailoring the pore size and incorporating a reactive transition metal ion toward a peroxide-free movement of the micromotors. Owing to the remarkably low costs and nonharmful nature,[20a] the zeolite motors can be considered as “disposable micromachines.” Yet, when necessary, these motors could be recovered by incorporating a magnetic layer (this would also allow magnetic guidance). The new concept is aimed not only towards environmental samples but largely towards efficient neutralization of stockpiles (e.g., barrels) of chemical or biological agents (CBWA), where the use of peroxide is not a concern and is actually widely used. Actually, most of the decontamination protocols developed by the US military for the detoxification of CBWA (e.g., Decon Green and DF200) rely on higher H_2O_2 levels of 35% and 8%, respectively.[41] While peroxide-driven motors are used here for proof-of-concept of the zeolite motors for catalytic detoxification of (bio) chemicalCBWA threats, environmental applications of such moving zeolite devices involving natural water media would require the use of alternative fuels. In particular, recently introduced water-based micromotors[19e,f] would allow for the movement of zeolite motors using the water sample itself as an in situ fuel. Alternatively, the concept can be applied using fuel-free zeolite micromotors (based on ultrasound or magnetic propulsion). The versatility of the zeolite-micromotor system is thus expected to enhance the efficiency and speed of detoxification processes of a broad range of chemical and biological threats present in a variety of matrices.

4. Experimental Section

Synthesis of Ag-Z Micromotors: The cubic Ag-exchanged zeolite (Ag-Z) Janus micromotors were prepared using zeolite (<45 µm; Sigma-Aldrich, USA) as the base particles. Ag-Z was prepared using a conventional ion-exchange procedure with an aqueous solution of silver nitrate (ACS reagent, ≥99.0%; Sigma–Aldrich, USA) at room temperature. The obtained Ag-Z was further processed by washing with distilled water and drying at 50 °C. After, ion-exchanged Ag-Z was cleaned in distilled water and subsequently filtered through an 8-µm filter membrane in order to get a uniform size. 100 µL of the Ag-Z was dispersed in isopropanol, which were then spread onto the glass slides and dried under room temperature. The cubes were coated with Ag layer using a Denton Discovery 18 sputter system. The deposition was performed at room temperature with a DC power of 200 W and an Ar pressure of 2.5 mT for 60 s. In order to obtain a uniform Janus half-shell coating, rotation was turned off and the sample slides were set up at an angle to be parallel to the Ag target. For the Al_2O_3-Ag-Z micromotors in the control experiments, the Al_2O_3 layer was deposited by ALD (Beneq TFS200) at 100 °C for 120 cycles on Ag-Z. The sputtering steps were the same as for the fabrication of the Ag-Z micromotors.

Propulsion of Janus Motor: The propulsion of zeolite micromotors in aqueous solution was performed by adding a solution containing 1% SDS (Sigma–Aldrich, USA) and 2% hydrogen peroxide (Sigma–Aldrich, USA). Videos were captured by an inverted optical microscope (Nikon Eclipse Instrument Inc. Ti-S/L100), coupled with a 20× and 10× objectives, a Hamamatsu digital camera C11440 and NIS Elements AR 3.2 software. The speed of the micromotors was tracked using a NIS Elements tracking module.

Spectrophotometric Measurement of Chemical Warfare Agent Simulant Diethyl Cholorophospahte: All of the measurements were performed with a UV–vis spectrophotometer (UV-2450, SHIMADZU). For adsorptive detoxification experiment, DCP was determined by monitoring the absorption curves of flouresceinamine isomer I (Aldrich, USA). The 0.5×10^{-3} M aqueous solution of flouresceinamine isomer I gives an absorption peak at 475 nm. In the presence of DCP, flouresceinamine isomer I will react and make an adduct, which results in a decrease in the absorbance of flouresceinamine isomer I. By measuring the decrease in absorbance signal flouresceinamine isomer I, the amount of DCP can be calculated. For adsorptive detoxification experiments, DCP was taken in 1 mL aqueous solution containing different amounts of Ag-Z micromotors (1×10^6 to 5×10^6 motors mL^{-1}) with 1% SDS and 2% hydrogen peroxide as propulsion medium. Samples were filtered before the spectrophotometric measurements to avoid possible interferences of the motors or their generated bubbles. After the remediation (adsorptive detoxification experiments), the reaction mixture was allowed to react with fluoresceinamine isomer I, after a 6-min duration, the absorbance was monitored and the decrease in absorbance signal at 475 nm is directly proportional to the amount of remaining DCP in the contaminated solution.

E. Coli Experiments: *Escherichia coli* (*E. coli*) bacteria (strain DH5α) were cultured in Luria broth (LB) agar overnight at 37 °C. Then, a single colony was inoculated into LB medium. Following the inoculation, the medium was cultured in a rotary shaker at 37 °C for 10 h and then refreshed with LB medium at 1:100 dilutions. The culture continued for another 3 h until the medium OD600 reached approximately 1.0, indicating the logarithmic growth phase. Aliquots of bacteria at a concentration of 9.2×10^9 cells mL^{-1} were stored at −25 °C until use. 1×10^8 cells mL^{-1}*E. coli* are used for the antibacterial experiments. After the experiment, the silver-exchanged zeolite micromotors were removed and then *E. coli* were centrifuged again at 14 000 rpm for 10 min to take away the supernatant. To check the efficiency of silver-exchanged zeolite micromotor, 1×10^8 cell mL^{-1} *E. coli bacteria* were taken into 1 mL aqueous solution containing to 5×10^6 motors mL^{-1} with 1% SDS and 2% hydrogen peroxide as propulsion medium. The reaction mixture was allowed to react for 6 min, and after that the micromotors were precipitated at 500 rpm for 1 min, and the supernatant (containing viable and nonviable *E. coli* cells) was centrifuged again at 14 000 rpm to make a bacterial pellet. The pellet was resuspended in 100 µL of a solution of Syto-9 dye and propidium iodide dye previously dissolved in water following specifications of the L13152LIVE/DEADBacLight bacterial viability kit provider. Eppendorfs were covered with aluminum foil and gently mixed for 20 min. A cleaning step was performed in order to remove unreacted dye. Furthermore, they were centrifuged at 14 000 rpm for 10 min and the pellet was resuspended in 100 µL of water for counting. Pictures of 2 µL drops were taken and the number of viable and nonviable cells was estimated by using the program ImageJ.

XRD and FT-IR Studies: XRD spectra were obtained using a Rotaflex RU-200B (Rigaku) with a 12-kW rotating Cu-anode source. FTIR spectra were collected in the range from 3500 to 700 cm^{-1} using a Nicolet 6700 spectrometer (Thermo Scientific).

Supporting Information

Supporting Information is available from the Wiley Online Library or from the author.

Acknowledgements

This project received support from the Defense Threat Reduction Agency-Joint Science and Technology Office for Chemical and Biological Defense (Grant no. HDTRA1–13–1–0002) and the UCSD Calit2 Strategic Research Opportunities (CSRO) Program. B. J.-S. acknowledges support from the EU 7th Framework 2007–2013 Program (Marie Curie Actions; Grant PIOF-GA-2012–326476).

Received: January 4, 2015
Revised: January 30, 2015
Published online: February 20, 2015

---

[1] a) Y. C. Yang, J. A. Baker, J. A. Ward, *Chem. Rev.* **1992**, *92*,1729; b) J. A. F. Compton, *Military chemical and biological agents, in: Chemical and Toxicological Properties*, The Telford Press, Caldwell, NJ **1987**.

[2] R. D. Albright, *Cleanup of Chemical and Explosive Munitions*, William Andrew, Norwich **2008**.

[3] D. E. Wilcox, *Chem. Rev.* **1996**, *96*, 2435.

[4] D. B. Kim, B. Gweon, S. Y. Moon, W. Choe, *Curr. Appl. Phys.* **2009**, *9*, 1093.

[5] A. V. Vorontsov, A. A. Panchenko, E. N. Savinov, C. Lion, P. G. Smirniotis, *Environ. Sci. Technol.* **2002**, *36*, 5261.

[6] *National Research Council Review and Evaluation of Alternative Chemical Disposal Techniques*, National Academy Press, Washington, DC **1996**.

[7] M. R. Seger, G. E. Maciel, *Environ. Sci. Technol.* **2006**, *40*, 797.

[8] M. R. Seger, G. E. Maciel, *Environ. Sci. Technol.* **2006**, *40*, 791.

[9] K. Knagge, M. Johnson, V. H. Grassian, S. C. Larsen, *Langmuir* **2006**, *22*, 11077.

[10] K. Kim, O. G. Tsay, D. A. Atwood, D. G. Churchill, *Chem. Rev.* **2011**, *111*, 5345.

[11] G. W. Wagner, P. W. Bartram, *Langmuir* **1999**, *15*, 8113.

[12] a) S. W. Yang, D. C. Doetschman, J. T. Schulte, J. B. Sambur, C. W. Kanyi, J. D. Fox, C. O. Kowenje, B. R. Jones, N. D. Sherma, *Microporous Mesoporous Mater.* **2006**, *92*, 56; b) Q. Meng, D. C. Doetschman, A. K. Rizos, M. H. Lee, J. T. Schulte, A. Spyros, C. W. Kanyi, *Environ. Sci. Technol.* **2011**, *45*, 3000.

[13] C. Damm, M. Neumann, H. Munstedt, *Soft Mater.* **2006**, *3*, 71.

[14] P. Gunawan, C. Guan, X. Song, Q. Zhang, S. S. J. Leong, C. Tang, Y. Chen, M. B. Chan-park, M. W. Chang, K. Wang, R. Xu, *ACS Nano* **2011**, *5*, 10033.

[15] K. Malachova, P. Raus, Z. Rybkova, O. Kozak, *Appl. Clay Sci.* **2011**, *53*, 642.

[16] Z. Li, D. Lee, X. Sheng, E. Robert, M. F. Rubner, *Langmuir* **2006**, *22*, 9820.

[17] A. Sokolov, R. Goldstein, F. Feldchtein, I. Aranson, *Phys. Rev. E* **2009**, *80*, 0310903.

[18] a) D. Patra, S. Sengupta, W. Duan, H. Zhang, R. Pavlick, A. Sen, *Nanoscale* **2013**, *5*, 1273; b) J. Wang, W. Gao, *ACS Nano* **2012**, *6*, 5745; c) J. Wang, *Nanomachines: Fundamentals and Applications*, Wiley-VCH, Weinheim, Germany **2013**, ISBN 978–3–527–33120–8; d) M. Guix, C. Carmen, C. C. Mayorga-Martinez, A. Merkoçi, *Chem. Rev.* **2014**, *114*, 6285.

[19] a) W. Gao, J. Wang, *ACS Nano* **2014**, *8*, 3170; b) L. Soler, S. Sanchez, *Nanoscale* **2014**, *6*, 7175; c) J. Orozco, G. Cheng, D. Vilela, S. Sattayasamitsathit, R. Vazquez-Duhalt, G. Valdes-Ramirez, O. S. Pak, A. Escarpa, C. Kan, J. Wang, *Angew. Chem. Int. Ed.* **2013**, *52*, 13276; d) L. Soler, V. Magdanz, V. M. Fomin, S. Sanchez, O. G. Schmidt, *ACS Nano* **2013**, *7*, 9611; e) W. Gao, X. Feng, A. Pei, Y. Gu, J. Li, J. Wang, *Nanoscale* **2013**, *5*, 4696; f) J. Li, V. V. Singh, S. Sattayasamitsathit, J. Orozco, K. Kaufmann, R. Dong, W. Gao, B. Jurado-Sanchez, Y. Fedorak, J. Wang,. *ACS Nano* **2014**, *8*, 11118; g) B. Jurado-Sanchez, S. Sattayasamitsathit, W. Gao, L. Santos,

Y. Fedorak, V. V. Singh, J. Orozco, M. Galarnyk, J. Wang, *Small* **2015**, *11*, 499; h) J. G. S. Moo, M. Pumera, *Chem. Eur. J.* **2015**, *21*, 58.
[20] a) M. M. Khin, A. S. Nair, V. J. Babu, R. Murugan, S. Ramakrishna, *Energy Environ. Sci.* **2012**, *5*, 8075; b) B. Dong, S. Belkhair, M. Zaarour, L. Fisher, J. Verran, L. Tosheva, R. Retoux, J.-P. Gilson, S. Mintova, *Nanoscale* **2014**, *6*, 10859; c) Y. Zhou, Y. Deng, P. He, F. Dong, Y. Xia, Y. He, *RSC Adv.* **2014**, *4*, 5283.
[21] T. Alava, N. B. Duroure, C. Ayela, E. Trevisol, M. Pungniere, Y. Morel, P. Rameil, L. Nicu, *Sens. Actuators B: Chem.* **2009**, *138*, 532.
[22] H. Wang, G. Zhao, M. Pumera, *J. Am. Chem. Soc.* **2014**, *136*, 2719.
[23] E. M. Anastasi, T. D. Wohlsen, H. M. Stratton, M. Katouli, *Water Res.* **2013**, *47*, 6670.
[24] G. D. Cremer, Y. Antoku, M. B. J. Roeffaers, M. Sliwa, J. V. Noyen, S. Smout, J. Hofkens, D. E. De Vos, B. F. Sels, T. Vosch, *Angew. Chem. Int. Ed.* **2008**, *47*, 2813.
[25] a) N. H. Fletcher, *J. Chem. Phys.* **1958**, *29*, 572; b) J. Li, G. Huang, M. Ye, M. Li, R. Liu, Y. Mein, *Nanoscale* **2011**, *3*, 5083; c) M. Manjare, B. Yang, Y. P. Zhao, *Phys. Rev. Lett.* **2012**, *109*, 128305; d) W. Huang, M. Manjare, Y. Zhao, *J. Phys. Chem. C* **2013**, *117*, 21590.
[26] Y. C. Yang, *Acc. Chem. Res.* **1999**, *32*, 109.
[27] W. D. Harkins, G. Jura, *J. Am. Chem. Soc.* **1944**, *66*, 1366.
[28] M. A. A. Musa, C. Y. Yin, R. M. Savory, *J. Appl. Sci.* **2011**, *11*, 3650.
[29] D. W. Breck, *Zeolite Molecular Sieves*, Robert E. Krieger, Malabar, FL **1984**, p.34.
[30] M. Sanchez-Polo, J. R. Utrill, E. Salhi, U. V. Gunten, *Water Res.* **2007**, *41*, 1031.
[31] G. W. Wagner, P. W. Bartram, O. Koper, K. J. Klabunde, *J. Phys. Chem. B* **1999**, *103*, 3225.
[32] P. A. Kolinko, D. V. Kozlov, *Environ. Sci. Technol.* **2008**, *42*, 4350.
[33] K. D. Demadis, S. S. Katarachia, *Phosphorus Sulfur Silicon* **2004**, *179*, 627.
[34] K. Malachova, P. Praus, Z. Rybkova, O. Kozak, *Appl. Clay Sci.* **2011**, *53*, 642.
[35] W. B. Hugo, *Int. Biodeter. Biodegr.* **1991**, *27*, 185.
[36] X. C. Li, L. Cai, C. D. Wu, *Phytochemistry* **1997**, *46*, 97.
[37] D. Russell, W. B. Hugo, *Prog. Med. Chem.* **1994**, *31*, 351.
[38] Y. Inoue, Y. Kanzaki, *J. Inorg. Biochem.* **1997**, *67*, 377.
[39] R. B. Thurman C. P. Gerba, *CRC Crit. Rev. Environ. Contam.* **1989**, *18*, 295.
[40] Y. Matsumura, K. Yoshikata, S. Kunisaki, T. Tetsuaki-Tsuchido, *Appl. Environ. Microbiol.* **2003**, *69*, 4278.
[41] G. W. Wagner, *Ind. Eng. Chem. Res.* **2011**, *50*, 12285.